Progress In Electromagnetics Research C, Vol. 96, 215–227, 2019

Gain Equalized Three Antenna Pattern Diversity Module for WLAN Access Points

Somanatha P. Swapna*, Gulur S. Karthikeya, Shiban K. Koul, and Ananjan Basu

Abstract—This paper demonstrates a three-port coaxial fed antenna system for wireless local area network (WLAN) access points, consisting of two dipoles and a patch, radiating at 5.2 GHz with impedance bandwidth of 150 MHz. The antennas are designed for pattern diversity in the end-fire and broadside orientation with an individual gain of 4.5 dBi, which is further enhanced to 6 dBi after integrating with unit-cell structures. The gain enhancement for individual antennas is achieved by strategically integrating transmission type and reflective type sub-wavelength structures for patch and dipoles, respectively. The realized ground plane is shared among the three antennas. The measured results show that the return loss of the antennas is unaffected by the unit-cell loading and has an isolation of less than 26 dB throughout the band and across the ports for a port-to-port distance of 0.25λ.

1. INTRODUCTION

State of the art wireless communication systems prefer GSM, WLAN, and Wi-MAX applications due to high-speed data transfer between mobile and stationary transceiver radios [1]. Dynamic wireless links are established in the case of mobile systems while communicating with ground base stations [2]. IEEE 802.11 is one of the most successful standards in wireless communication systems due to high throughput and low cost. WLAN antennas are often small and require an omnidirectional radiation pattern due to area limitations in wireless devices [3].

The capability to support multidirectional far-field radiation pattern is a fairly attractive feature in many communication systems. Equal gains are required for a multiport system to maintain a reasonable link budget for the required angular coverage [4]. Researchers in [5] proposed a three-port ring antenna with mutual coupling less than 20 dB where the exciting ports create omnidirectional and broadside radiation pattern for a pattern diversity antenna. The antenna provides only a 45° coverage on the boresight, and the omnidirectional pattern provides a low gain of 2.85 dBi. A three-port dielectric resonator antenna using three mutually decoupled and near-degenerate modes is proposed in [6]. A three-module polarization diversity cylindrical DRA was proposed in [7] at 2.4 GHz WLAN. However, it requires expensive high dielectric material. A three-port WLAN antenna for 2.4 GHz band with nearly full azimuth coverage with a low gain of 2.3 dBi per element is proposed in [8]. Researchers in [9] proposed a three-port antenna with azimuth and broadside coverage, but the gain of the antenna varies from 1 dBi to 3.8 dBi across the three ports. A compact multiband antenna covering MIMO, LTE, GPS, WLAN, and WAVE bands was proposed for automotive applications in [10]. But the high mutual coupling of the antenna does affect the overall performance. A circularly polarized high-gain planar dipole-array antenna for wireless local area networks applications is proposed in [11]. The large size of the antenna along with power divider circuit makes the overall design very intricate to deal with. A six-port multiple-input-multiple-output antenna system for 5-GHz WLAN access points application

Received 27 July 2019, Accepted 17 October 2019, Scheduled 3 November 2019
* Corresponding author: Somanatha Pai Swapna (s.swapna.pai@gmail.com).
The authors are with the Indian Institute of Technology Delhi, India.

is proposed in [12]. It has a good isolation performance, but the aperture coupled antennas mounted on a hollow metal structure backed by a quarter-wave-length choke make the antennas complex for the given functionality, and the gains of the different antennas also show a variation from 3.5 to 5 dBi. [13] proposed a dual-band dual-polarized dipole antenna with good anti-interference capability for 2.4-/5-GHz WLAN applications. But the design has a limited coverage of only 30° which can provide limited functionality for the designed applications. A miniaturized UWB antenna for WLAN with slitted EBG was proposed in [14]. But the antenna has a gain of 3.3 dBi which is low considering the WLAN application and provides a limited coverage of 30°. From the existing literature what we were able to conclude was that an antenna that could provide maximum angular coverage for a consistent high gain throughout the band and throughout different ports would provide a more desirable solution to WLAN applications, and such a design was lacking in the literature surveyed. We particularly focussed on the angular coverage as there was a probability that the signal could go undetected if the user went outside the coverage area.

This paper presents a three-element pattern diversity antenna system module for 5.2 GHz WLAN access points with less than 26 dB isolation. The objective is to maintain uniformity in the gain enhancement between the dipole and patch antennas that provide end-fire and broadside coverage respectively. The superstrate and sub-wavelength parasitic reflectors are designed for gain enhancement throughout the ports. The integrated module provides inexpensive fabrication with desirable characteristics of pattern diversity and minimal electrical footprint for WLAN.

2. ANTENNA DESIGN AND ANALYSIS

2.1. Three Element Antenna Design

The three-element antenna design consists of two dipoles at the two edges of the substrate along with a patch at the centre as shown in Fig. 1. The substrate used is Rogers RO4350B with dielectric constant $\epsilon_r = 3.66$ and 20 mil thickness. The low dielectric constant helps to maintain minimal surface wave modes. The thickness of 20 mil ensures proper mechanical stability to the antenna.

Initially, a conventional circular patch with coaxial feed is designed to model an antenna structure that is compact and optimized to operate at 5.2 GHz. A circular slot along with two rectangular slots is introduced in the patch to further improve the bandwidth of the antenna. The patch antenna is fed

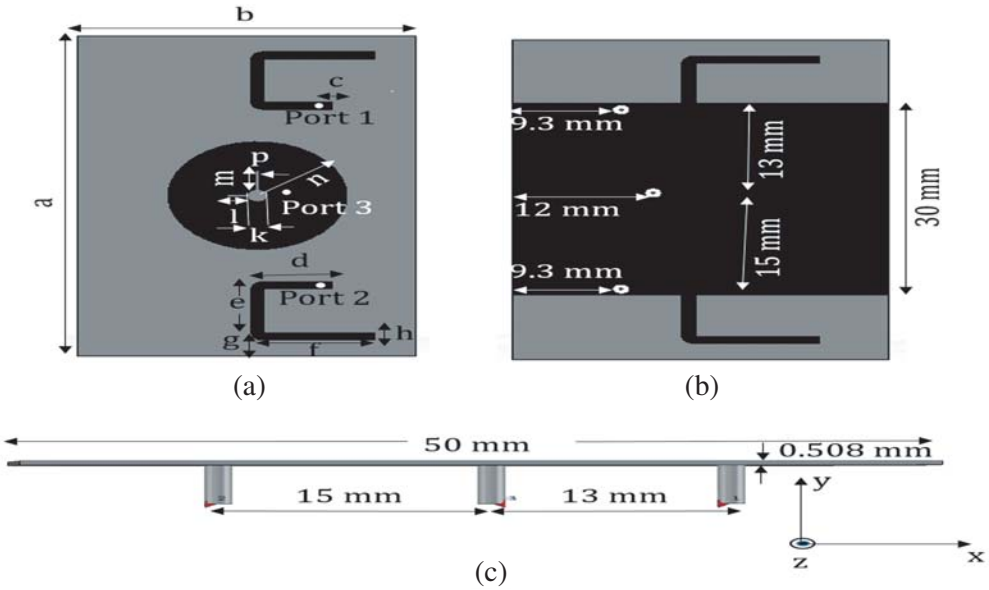

Figure 1. Schematic of three element antenna system, (a) top view, (b) bottom view, (c) side view [$a = 50$ mm, $b = 32$ mm, $c = 1.37$ mm, $d = 6.5$ mm, $e = 7$ mm, $f = 10.5$ mm, $g = 2.5$ mm, $h = 1.14$ mm, $k = 1.94$ mm, $l = 1.96$ mm, $m = 2.93$ mm, $n = 8.45$ mm, $p = 0.39$ mm].

using a coaxial feed which aids in an electrically compact design with high pattern integrity and helps in easier impedance matching [15]. Thereafter, the two dipoles are designed, and its two arms are printed on the opposite sides of the substrate along with a coaxial fed input. The feeding point for the three antennas is optimized for 50 Ω impedance matching at the operating frequency. The entire three port antenna system has an area of $32 \times 50\,\text{mm}^2 (0.56\lambda \times 0.9\lambda)$, where λ is the free-space wavelength with respect to 5.2 GHz. An adequate finite ground plane of dimension 30 mm × 32 mm ($0.52\lambda \times 0.56\lambda$) is provided at the bottom side of the substrate. The ground plane acts as a reflector and stabilizes the radiation pattern in the required frequency band. In this design, if we consider three dipoles in the three ports, the dipole at port 3 with inadequate ground plane will result in poor front-to-back ratio during antenna radiation. If we consider three patch antennas, the patches at port 1 and port 2 will not provide sufficient tilt for the patterns to cover the required area, unless the antennas are tilted physically which will make it a non-planar design. For a planar antenna to cover the required area, the solution is to use two dipoles for endfire coverage and a patch for broadside coverage.

The parametric study of the antenna to obtain the desired dimensions is as shown in Fig. 2. Fig. 2(a) shows the variation of the resonant frequency of the patch as the radius of the patch is increased ($n1$) and decreased ($n3$) from the optimum radius. Fig. 2(b) depicts the variation in the bandwidth of the patch when the radius of the inner slotted circle is changed. The patch shows two resonant modes when the dimension of k is increased ($k1$) and a lower bandwidth when k is reduced ($k3$). The optimum dimension ($k2$) gives the maximum bandwidth for the patch. Figs. 2(c) and (d) show how the resonant frequency is affected when the dimension of the dipole is varied. The length of the dipole must be approximately $\lambda/2$ at the resonant frequency ($f2, e2$). As inferred from the figure, when the length of the dipole is increased ($f1, e1$) the resonant frequency is reduced, and the resonant frequency increases when the length of the dipole is reduced ($f3, e3$). The antennas are initially optimized separately and then moved close to each other at the same time keeping a good mutual coupling between the antennas.

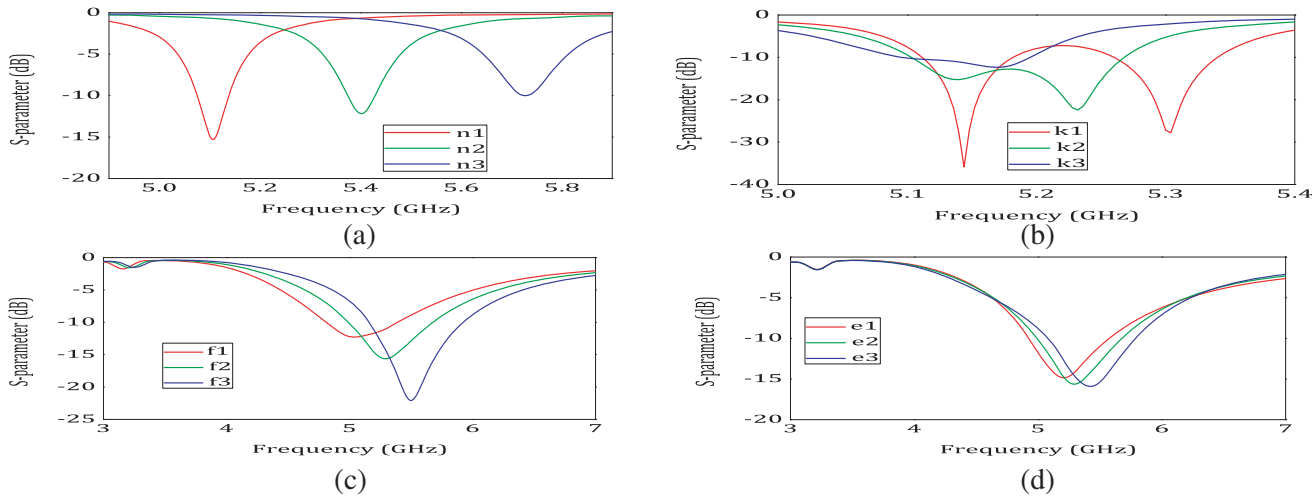

Figure 2. Parametric study of different dimensions of the antenna structure.

The equivalent circuit for the proposed antenna is represented in Fig. 3. The equivalent circuit model for the dipole [16] and the patch [17] is provided along with the impedance matching circuit [18] which is matched to 50 Ω input ports. The C_{0p} at the patch specifies the feed point impedance, and R_{0p} is the conduction loss of the substrate. The tank circuits of the patch and dipole antenna are frequency dependent which provides the resonance for the antenna. The mutual coupling between the antennas is modelled as the coupling capacitance between the dipole and patch antenna.

The basic mathematical formulation for the design of the antennas is obtained from [19]. Further, full-wave method of moments (MoM) analysis to understand the circular patch antenna is described in [20]. The modelling of a coaxially fed patch antenna is also described in [21]. The 50 Ω impedance matching for coaxial inputs for the dipole and patch is determined through parametric study of the

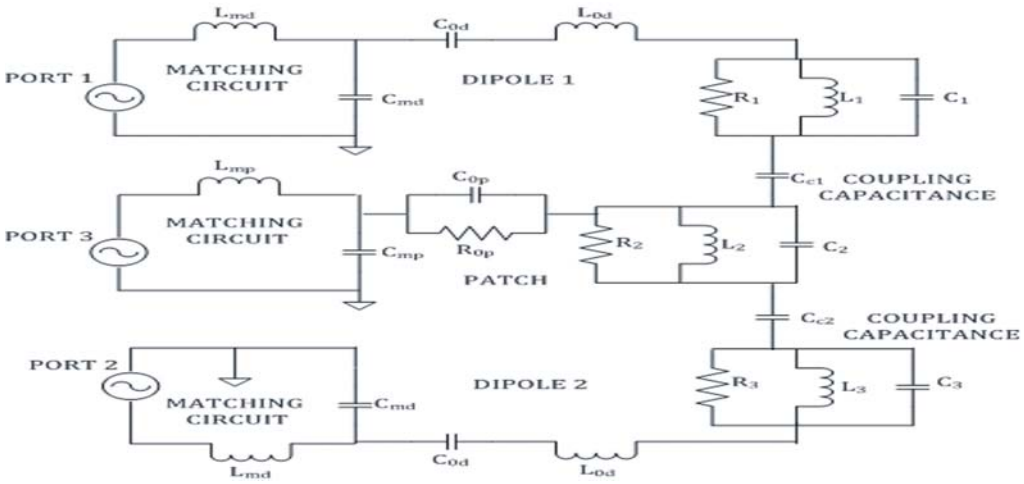

Figure 3. Equivalent circuit of the antenna.

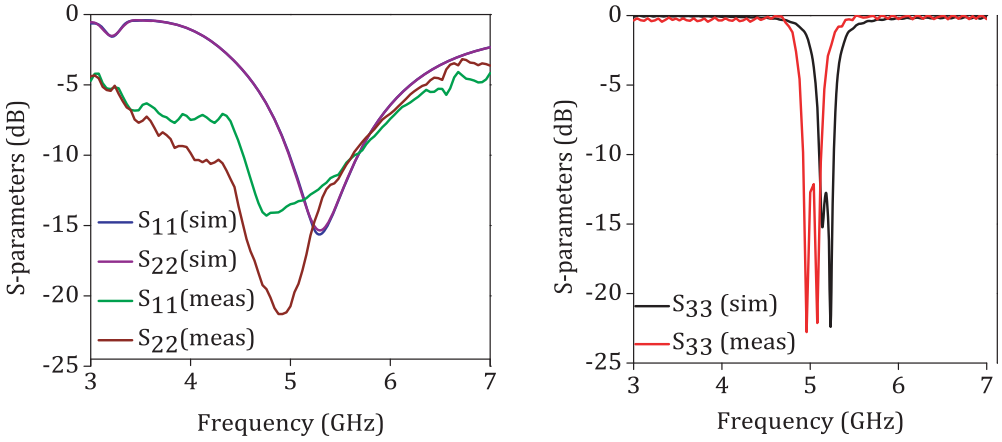

Figure 4. Input reflection coefficients of dipole and patch without unit-cell structures.

antennas.

The simulated and measured input reflection coefficients are shown in Fig. 4. The simulated impedance bandwidth for the antenna system is determined by the patch whose bandwidth is 150 MHz (5.10 GHz–5.26 GHz). The variation in bandwidth is because the bandwidth of S_{33} is determined by patch antenna which has a narrow bandwidth due to its inherent resonating nature compared to a dipole which determines the bandwidth for S_{11} and S_{22}. A frequency shift of 200 MHz between the simulated and measured resonances can be attributed to fabrication tolerances that introduce a small lead inductance resulting in an additional stepped impedance to the radiating element and the tolerance of substrate permittivity. Many communication systems such as WLAN do not require large instantaneous bandwidth and therefore prefer narrow-band antennas [22]. The half power beamwidth (HPBW) of the dipole is around 180° with a front-to-back ratio of 11 dB, and for the patch, it is around 100° and 15 dB, respectively. The dipole antennas on port 1 and port 2 radiate along endfire orientation and the patch radiates along the broadside with a gain of 4.5 dBi.

To enhance the gain of the antenna described in the previous section two different unit-cell structures are designed.

2.2. Design and Analysis of Unit-Cell 1

The unit-cell structure as shown in Fig. 5(a) is designed to improve characteristics of the patch antenna. The S-parameters from Fig. 5(b) show that it is a transmission type unit-cell structure. The substrate

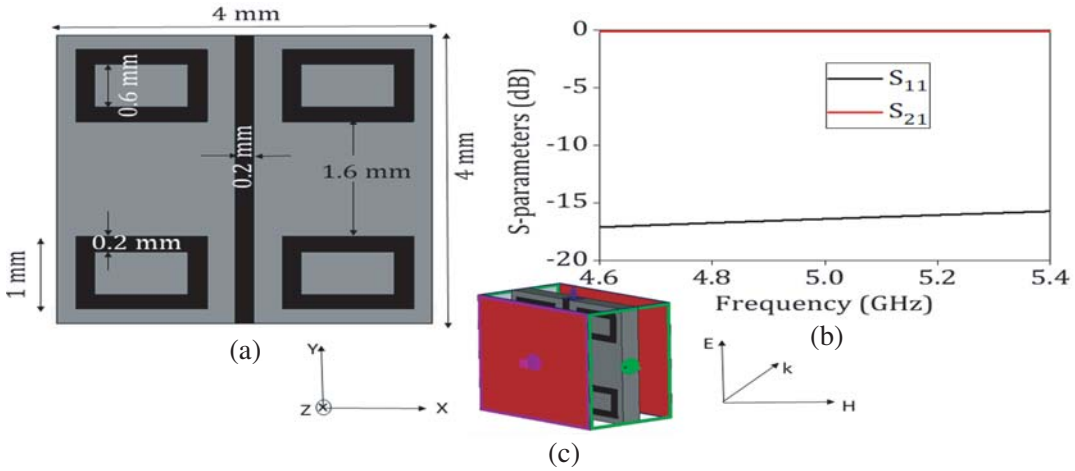

Figure 5. (a) Configuration of unit-cell 1. (b) S-parameters of the unit-cell. (c) The boundary conditions used for simulation.

used has a dielectric constant of $\epsilon_r = 3.66$ and is 0.508 mm thick.

To extract S-parameters as well as refractive index, PEC and PMC boundary conditions are assigned in the xz- and yz-planes of the proposed unit cell. The two ports are assigned in the z-direction. The parameters of the unit cell are extracted using the full-wave EM simulation software CST Microwave Studio. The magnitude S_{21} of the unit-cell at the operating frequency of 5.2 GHz is -0.1 dB. The high transmission characteristic of the unit-cell ensures a higher gain for the antenna by squeezing the radiation from the radiator below the metasurface into a narrow beam. The S_{11} magnitude of -16 dB makes sure that little power gets reflected back to the antenna by the unit-cell layers.

2.3. Design and Analysis of Unit-Cell 2

The unit-cell structure as shown in Fig. 6(a) is designed to improve the characteristics of the dipoles. The S-parameters from Fig. 6(b) show that it is a reflective type unit cell with a return loss of -1.2 dB at the operating frequency. The PEC and PMC boundary conditions are assigned in the xz- and yz-

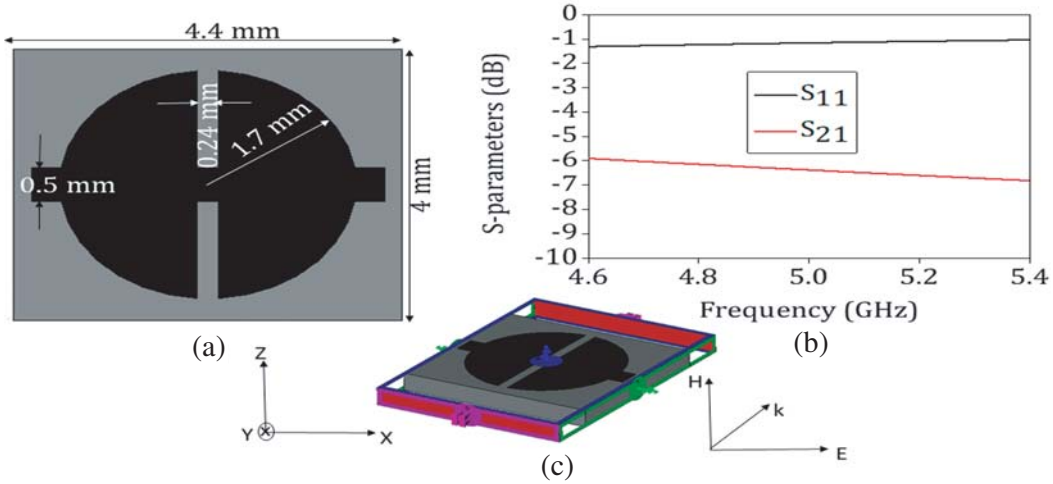

Figure 6. (a) Configuration of unit-cell 2. (b) S-parameters of the unit-cell. (c) The boundary conditions used for simulation.

planes of the proposed unit cell. The two ports are assigned in the y-direction. The magnitude S_{11} of the unit cell at the operating frequency of 5.2 GHz is -1 dB where the unit cell acts as a reflector. Also as the S_{21} magnitude is -6.6 dB, there is very little transmission of EM waves which helps in squeezing the radiation and improving the gain in forward direction.

The unit cells are strategically integrated with the earlier discussed antenna geometry and characterized along with the antenna design.

2.4. Proposed Three Element Antenna Design with Unit-Cell Structures

Figure 7 shows the proposed antenna along with the unit-cell structures. Initially, only a single layer of the unit cell 1 as in Fig. 8(a) is placed over the patch antenna, where the superstrate layer is maintained at a distance of 0.18λ. The unit cell 2 as in Fig. 8(b) is arranged beside the dipole antennas. There is gain improvement, but the gains of dipole and patch are equal only at a single frequency of 5.26 GHz. An additional layer of unit cell 1 is placed at a height of 0.04λ from the previous layer over the patch. The extra layer of unit cells makes the gain of three ports enhanced to 6 dBi over the entire bandwidth. The gain enhancement using Yagi-Uda directors and reflectors is significantly less than the gain enhancement obtained using the unit-cell structures. If the height of the superstrate is further increased, the gains of dipoles and the patch begin to decrease. If the superstrate is placed closer to the antennas, it is observed that the gain of the dipole is reduced. Compared to the superstrate design in [23], the proposed design

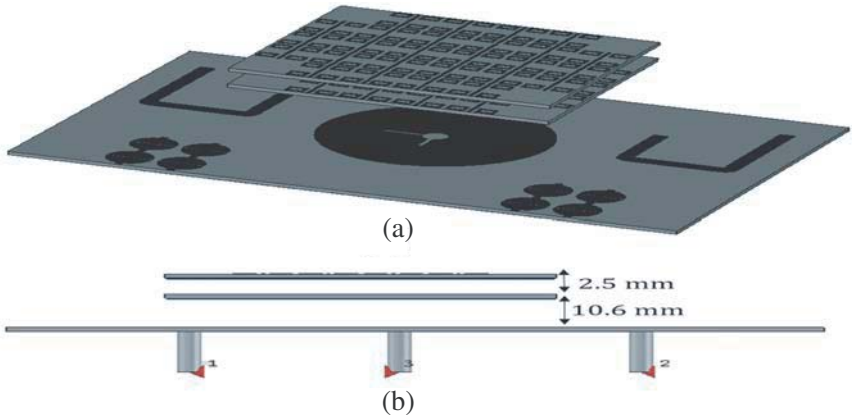

Figure 7. Configuration of the proposed three element antenna structure with unit-cells, (a) top view, (b) side view.

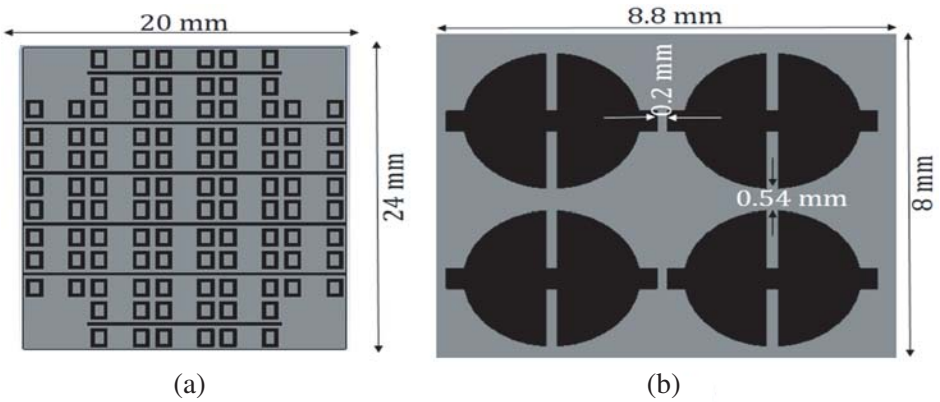

Figure 8. (a) Arrangement of the unit-cell 1 above the patch. (b) Arrangement of the unit-cell 2 beside the dipole.

is much more compact in terms of distance from the patch for a minimal gain variation between the antennas.

The electric field distributions before and after the unit-cell loading are shown in Fig. 9. For the dipole, the unit cell increases the electric field intensity towards the endfire side which demonstrates the reflective action of the unit cells. When the metasurface is mounted 0.22λ away from the patch, it aids in phase correction consequently leading to gain enhancement. The gap between the patch and the superstrate is significant because it has an influence on the gain of the patch as well as the dipole. The appended unit-cell structures aid in phase correction of the incoming cylindrical waves. The phase shifts contributed by the individual unit-cell structures are same which then adds up for the entire structure. The unit-cell structures will reflect the EM waves in phase at the resonant frequency which then aids in gain enhancement in the corresponding direction.

Here, the metasurface above the patch has a periodic, electrically small, unit-cell structures. In a material with positive permittivity and permeability, there is a delay in the phase of the wave as it moves forward [24]. By keeping a metasurface on the other side at a proper distance with an air gap, we can have the phase delay to be reversed such that the phase of the wave post the metasurface is the same as the phase of the wave at the patch antenna surface. This makes the wave radiate like a planar wave rather than a spherical like wave profile [25].

For each port, the simulated and measured input reflection coefficients are as shown in Fig. 10.

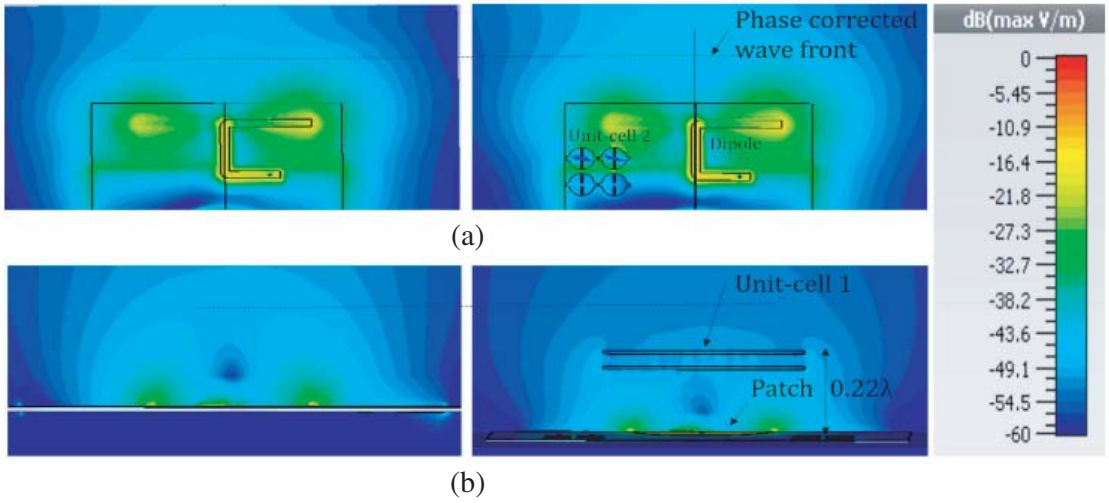

Figure 9. (a) Electric field distribution for the dipole. (b) Electric field distribution for the patch before and after the arrangement of unit-cells.

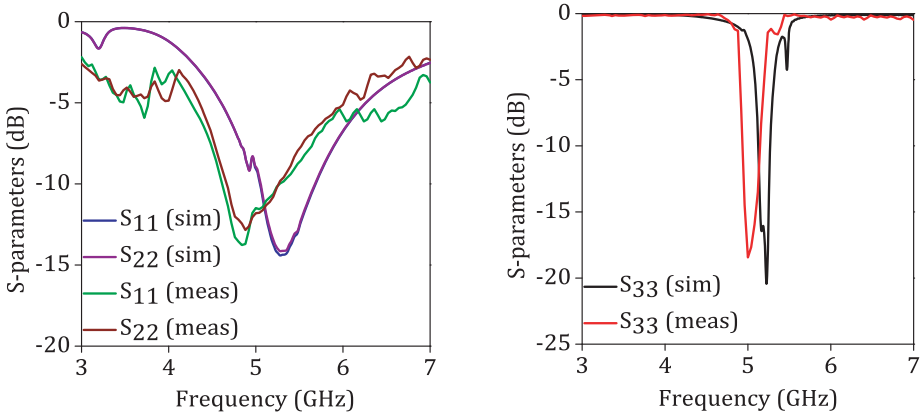

Figure 10. Input reflection coefficients of dipole and patch after unit-cell loading.

The simulated impedance bandwidth for the antenna system is 150 MHz (5.12 GHz–5.27 GHz) which presents the fact that there is no significant impedance bandwidth alteration after the integration by the unit cells. The simulated half power beamwidth (HPBW) of the dipoles is around 120° with a front-to-back ratio of 13 dB, and for patch it is around 90° and 11 dB, respectively.

The radiation patterns of the antenna in the E-plane before and after the unit-cell loading are shown in Fig. 11. The E-plane patterns show radiation at $\theta = 0°, +90°, -90°$. From the figure, we can infer that the radiation pattern is stable at the resonant frequency of the antenna. The beamwidth of the antenna after the unit-cell loading gets compressed compared to the patterns of the antenna before unit-cell loading due to increased gain. The cross polarization levels are much smaller over the operating frequency band for the dipole antennas. The circular patch is circularly polarized (LHCP) which can be inferred from similar co- and cross-polarization levels of the radiation patterns. There is good agreement between the simulated and measured radiation patterns, and slight variations are due to misalignments during measurement.

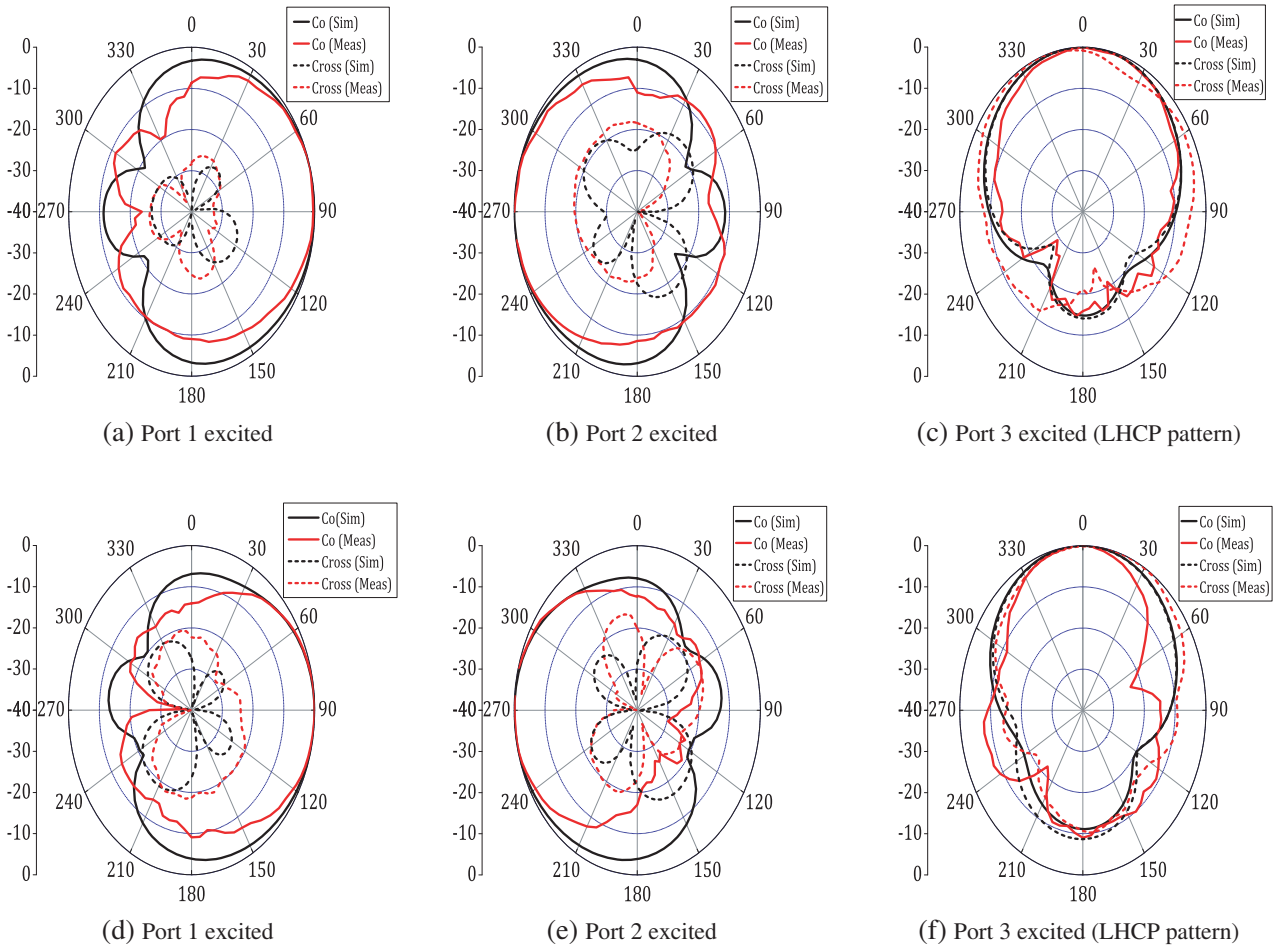

(a) Port 1 excited (b) Port 2 excited (c) Port 3 excited (LHCP pattern)

(d) Port 1 excited (e) Port 2 excited (f) Port 3 excited (LHCP pattern)

Figure 11. Radiation pattern at the operating frequency of 5.2 GHz (a), (b) and (c) before unit-cell loading and (d), (e), (f) after unit-cell loading.

To understand the behavior of the resonant mode of the proposed antenna, the simulated surface current distributions at 5.2 GHz are shown in Fig. 12. The surface current distribution is seen at dipoles when either port 1 or 2 is switched on and at the patch when port 3 is switched on. There is an increased magnitude in the surface current distribution post the integration with unit-cell structures. The surface current distribution of the dipole shows a high gain towards the endfire directions whereas the surface current distribution of the patch shows a high gain towards the broadside direction. Due to the coupling

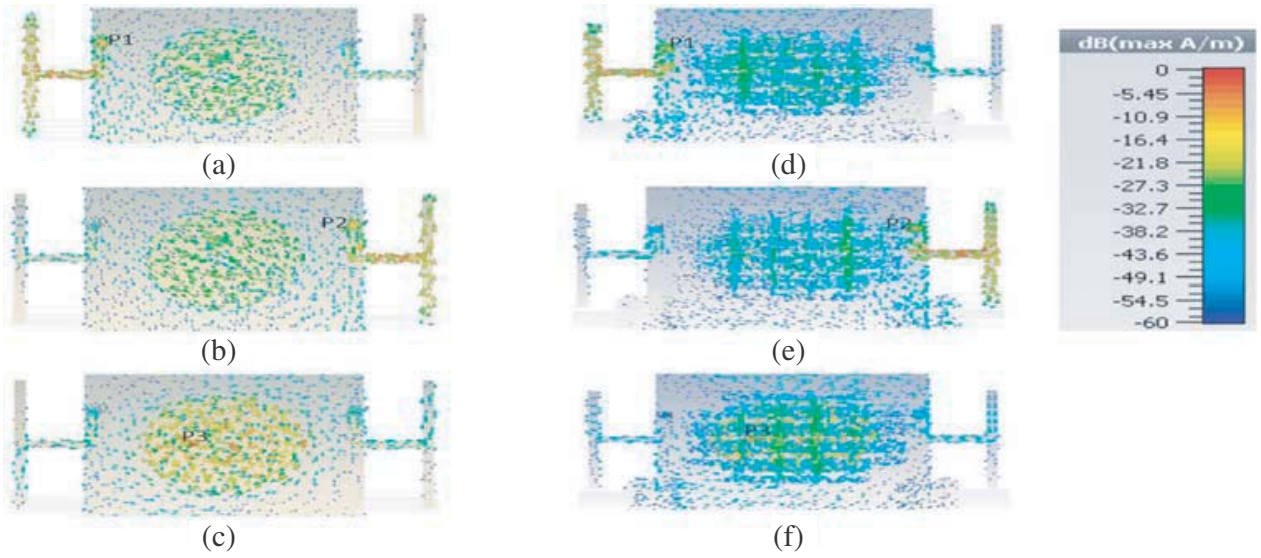

Figure 12. Surface current distribution of the antenna when (a) port 1, (b) port 2, (c) port 3 is excited before unit-cell loading and (d) port 1, (e) port 2, (f) port 3 is excited after unit-cell loading.

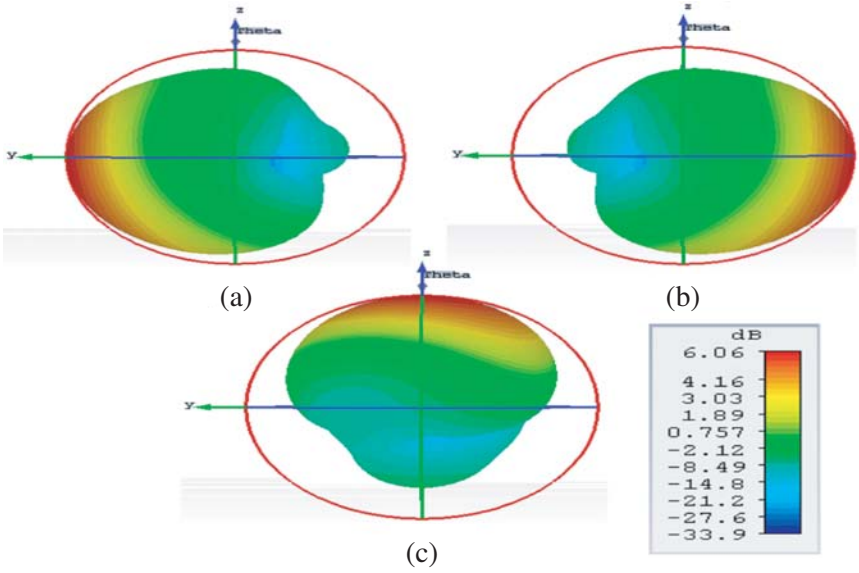

Figure 13. 3D-gain of the proposed antenna at 5.2 GHz when (a) port 1 is excited, (b) port 2 is excited, (c) port 3 is excited.

of energy from the antenna to the unit cells, the surface currents distribution of the antenna feed will be changed, and currents will be induced on the metasurface. As a result, the patch antenna acts as the primary microstrip feed while the metasurface is the real aperture that radiates energy to the free space.

Figure 13 shows the 3D-gain of the proposed antenna at the resonant frequency of 5.2 GHz when different ports are excited after the unit-cell integration. This indicates the direction of maximum radiation for different values of theta and phi. The maximum gain of 6 dBi for the antenna is at $0°, +90°$, and $-90°$. We can also infer that the directivity of the antennas is wide enough to provide coverage of $330°$ across the three ports.

The gain enhancement of the three ports is shown in Fig. 14(a) with a simulated gain of 6 dBi after the introduction of the unit-cell structures. Fig. 14(b) shows the simulated radiation pattern of the

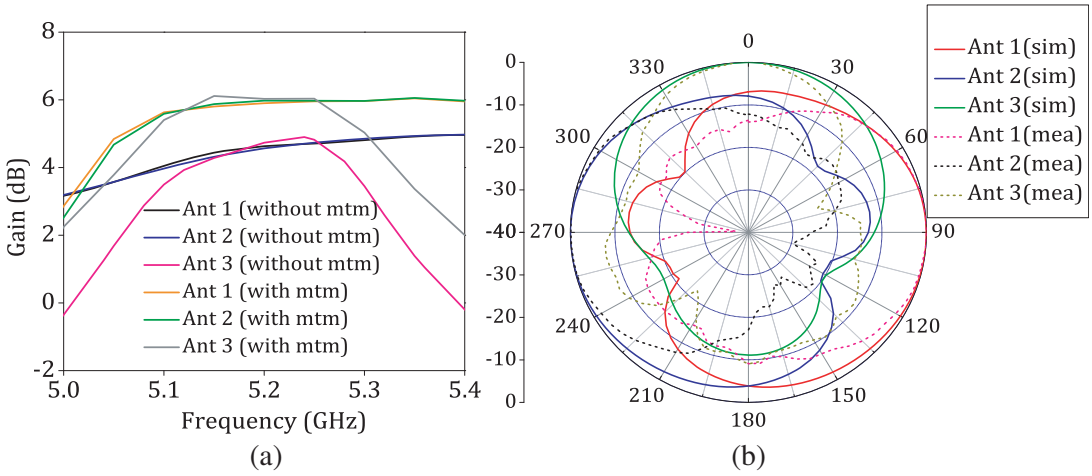

Figure 14. (a) Gain of the antenna without and with unit-cell structures. (b) Angular coverage of the proposed antenna at 5.2 GHz.

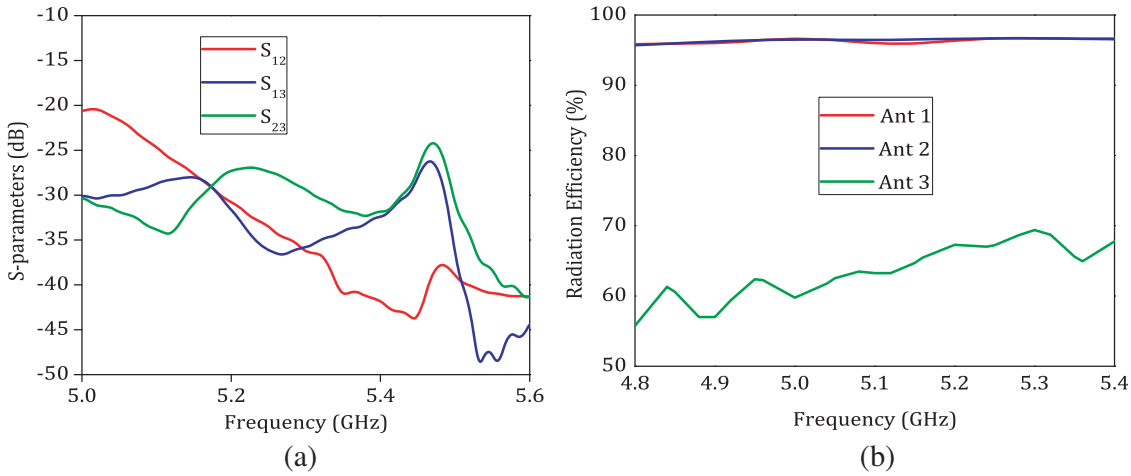

Figure 15. (a) Mutual coupling. (b) Radiation efficiency.

proposed antenna and how it covers 330° around the antenna structure, making it suitable for WLAN applications. The antennas maintain an isolation of 26 dB at the operating frequency for an electrical distance of 0.25λ between the ports as shown in Fig. 15.

Figure 16 depicts photographs of the fabricated prototype of the antenna design without and with unit-cell structures. Three SMA connectors are connected to input ports of the antenna. The reflection coefficient of the antenna is measured using Anritsu MS2028C Vector Network Analyser, and the far field measurements are conducted inside an anechoic chamber. At a time a single port is excited, and the other ports are terminated with a 50 Ω load. The gain transfer method is used for measuring the gain of the antenna. An ETS-Lindgreen 3115 Model double ridged waveguide horn antenna is used as the standard gain antenna for the measurement. There is a reasonable agreement between the simulation and measurement results, and the slight discrepancies are due to the connector soldering and fabrication tolerances which were not taken into account during simulation.

The performance of the antenna is compared with the existing three element antenna designs, and it is tabulated in Table 1. The proposed antenna provides higher gain with a wider angular coverage and is electrically compact as designed for WLAN antennas.

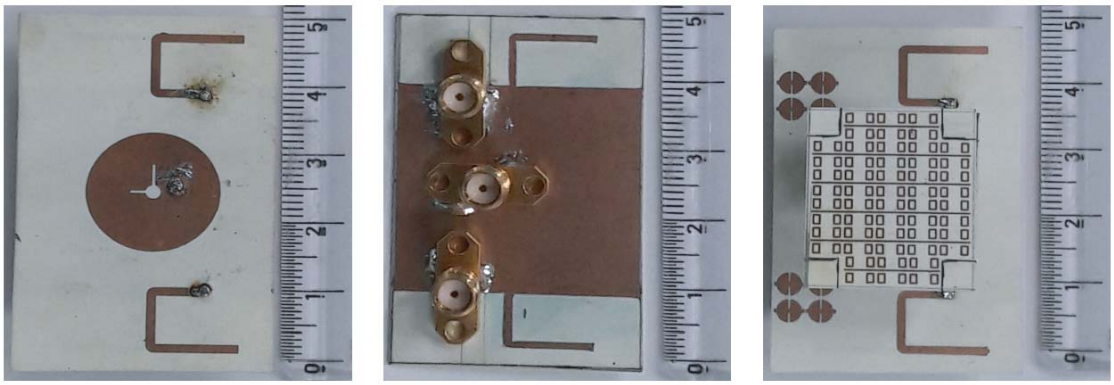

(a) (b) (c)

Figure 16. Photograph of the fabricated antenna, (a) top view before unit-cell loading, (b) bottom view, (c) top view after the unit-cell loading.

Table 1. Comparison of the proposed structure.

Ref	Freq (GHz)	Operating range (GHz)	No. of bands covered	Size	Pattern diversity	Coverage	Isolation (dB)	Radiation Efficiency (%)	Gain (dBi)
[5]	2.5	2.57–2.64	1	$0.62\lambda \times 0.62\lambda \times 0.25\lambda$	Ominidirectional and Broadside	120°	20	48, 85, 95	2.8
[9]	5.8	5.67–5.91	1	$0.92\lambda \times 0.58\lambda$	Broadside and endfire	180°	18	50, 85, 85	2.0
[26]	2.6	2.57–2.64	1	$1.04\lambda \times 1.04\lambda \times 0.1\lambda$	$+20°, -20°$	40°	-	41, 46	6.0
[27]	3.1	3.10–11.5	UWB	$0.5\lambda \times 0.25\lambda$	$0°, +90°, -90°$	120°	18	70, 80, 85	2.5
[28]	2.44	2.42–2.5	1	$0.8\lambda \times 0.48\lambda$	$+90°, -90°$	120°	20	44, 51	0.3
[29]	5.8	5.5–6.3	1	$0.6\lambda \times 0.5\lambda$	Broadside, Endfire	120°	13	96, 96	2.5
[30]	5.0	2.87–16.56	UWB	$0.38\lambda \times 0.38\lambda$	Conical patterns only	30°	-	70	7
[31]	5.8	2.54–15.36	UWB	$0.32\lambda \times 0.32\lambda$	Conical patterns only	30°	-	76	3
PA	**5.2**	**5.12–5.27**	**1**	$\mathbf{0.56\lambda \times 0.9\lambda \times 0.18\lambda}$	**Broadside, Endfire**	**330°**	**26**	**96, 96, 67**	**6.0**

PA = Proposed antenna

3. CONCLUSION

A gain equalized three-port antenna with pattern diversity for WLAN access points is proposed in this paper. Gain enhancement is achieved by loading two different unit-cell structures. The measurements show that the three-port unit-cell-loaded antenna presents a wide angular coverage of 330° in the operating frequency (5.2 GHz) with a gain of 6 dBi. The gain equivalence of different ports and a compact structure make this antenna beneficial in wireless systems.

REFERENCES

1. Kim, J. and I. Lee, "802.11 WLAN: History and new enabling MIMO techniques for next generation standards," *IEEE Communications Magazine*, Vol. 53, No. 3, 134–140, Mar. 2015.

2. Jaeck, V., L. Bernard, K. Mahdjoubi, R. Sauleau, S. Collardey, P. Pouliguen, and P. Potier, "A conical patch antenna array for agile point-to-point communications in the 5.2-GHz band," *IEEE Antennas and Wireless Propagation Letters*, Vol. 15, 1230–1233, Dec. 2016.
3. Bartz, R. J., *Mobile Computing Deployment and Management: Real World Skills for CompTIA Mobility Certification and Beyond*, Wiley, 2015.
4. Chou, H. and H. Su, "Dual-band hybrid antenna structure with spatial diversity for DTV and WLAN applications," *IEEE Transactions on Antennas and Propagation*, Vol. 65, No. 9, 4850–4853, Sep. 2017.
5. Saurav, K., N. K. Mallat, and Y. M. M. Antar, "A three-port polarization and pattern diversity ring antenna," *IEEE Antennas and Wireless Propagation Letters*, Vol. 17, No. 7, 1324–1328, Jul. 2018.
6. Abdalrazik, A., A. S. A. El-Hameed, and A. B. Abdel-Rahman, "A three-port MIMO dielectric resonator antenna using decoupled modes," *IEEE Antennas and Wireless Propagation Letters*, Vol. 16, 3104–3107, 2017.
7. Fang, X. S., K. W. Leung, and K. M. Luk, "Theory and experiment of three-port polarization-diversity cylindrical dielectric resonator antenna," *IEEE Transactions on Antennas and Propagation*, Vol. 62, No. 10, 4945–4951, Oct. 2014.
8. Wang, H., L. Liu, Z. Zhang, Y. Li, and Z. Feng, "Ultra-compact three-port MIMO antenna with high isolation and directional radiation patterns," *IEEE Antennas and Wireless Propagation Letters*, Vol. 13, 1545–1548, 2014.
9. Sharma, Y., D. Sarkar, K. Saurav, and K. V. Srivastava, "Three-element MIMO antenna system with pattern and polarization diversity for WLAN applications," *IEEE Antennas and Wireless Propagation Letters*, Vol. 16, 1163–1166, 2017.
10. Kwon, O., R. Song, and B. Kim, "A fully integrated shark-fin antenna for MIMO-LTE, GPS, WLAN, and wave applications," *IEEE Antennas and Wireless Propagation Letters*, Vol. 17, No. 4, 600–603, Apr. 2018.
11. Kim, S. and J. Kim, "A circularly polarized high-gain planar 2×2 dipole-array antenna fed by a 4-way Gysel power divider for wlan applications," *IEEE Antennas and Wireless Propagation Letters*, Vol. 18, No. 5, 1051–1055, May 2019.
12. Han, W., X. Zhou, J. Ouyang, Y. Li, R. Long, and F. Yang, "A six-port mimo antenna system with high isolation for 5-GHz WLAN access points," *IEEE Antennas and Wireless Propagation Letters*, Vol. 13, 880–883, 2014.
13. Zhang, Y., Y. Zhang, D. Li, K. Liu, and Y. Fan, "Dual-polarized band-notched antenna without extra circuit for 2.4/5 GHz WLAN applications," *IEEE Access*, Vol. 7, 84 890–84 896, 2019.
14. Ghahremani, M., C. Ghobadi, J. Nourinia, M. S. Ellis, F. Alizadeh, and B. Mohammadi, "Miniaturised UWB antenna with dual-band rejection of WLAN/WiMAX using slitted EBG structure," *IET Microwaves, Antennas Propagation*, Vol. 13, No. 3, 360–366, 2019.
15. Bhartia, P., I. Bahl, R. Garg, and A. Ittipiboon, *Microstrip Antenna Design Handbook (Artech House Antennas and Propagation Library)*, ser. Artech House Antennas and Propagation Library, Artech House Publishers, 2000.
16. Hamid, M. and R. Hamid, "Equivalent circuit of dipole antenna of arbitrary length," *IEEE Transactions on Antennas and Propagation*, Vol. 45, No. 11, 1695–1696, Nov. 1997.
17. Ansarizadeh, M., A. Ghorbani, and R. A. Abd-Alhameed, "An approach to equivalent circuit modeling of rectangular microstrip antennas," *Progress In Electromagnetics Research B*, Vol. 8, 77–86, 2008.
18. Pozar, D. M., *Microwave Engineering*, 3rd Edition, Wiley, Hoboken, NJ, 2005.
19. Balanis, C. A., *Antenna Theory: Analysis and Design*, Wiley-Interscience, 2005.
20. Latif, S. I. and L. Shafai, "Pattern equalization of circular patch antennas using different substrate permittivities and ground plane sizes," *IEEE Transactions on Antennas and Propagation*, Vol. 59, No. 10, 3502–3511, Oct. 2011.
21. Wu, C., K. Wu, Z. Bi, and J. Litva, "Modelling of coaxial-fed microstrip patch antenna by finite difference time domain method," *Electronics Letters*, Vol. 27, No. 19, 1691–1692, Sep. 1991.

22. Waterhouse, R., *Printed Antennas for Wireless Communications*, 1st edition, ser. RSP, Wiley, 2007.
23. Kim, J. H., C. Ahn, and J. Bang, "Antenna gain enhancement using a holey superstrate," *IEEE Transactions on Antennas and Propagation*, Vol. 64, No. 3, 1164–1167, Mar. 2016.
24. Engheta, N., "An idea for thin subwavelength cavity resonators using metamaterials with negative permittivity and permeability," *IEEE Antennas and Wireless Propagation Letters*, Vol. 1, 10–13, 2002.
25. Y. F. B. Z. J. Z. Ke Chen, Z. Yang, and T. Jiang, "Improving microwave antenna gain and bandwidth with phase compensation metasurface," *AIP Advances*, Vol. 5, No. 6, 1695–1696, Jun. 2015.
26. Naqvi, A. H. and S. Lim, "A beam-steering antenna with a fluidically programmable metasurface," *IEEE Transactions on Antennas and Propagation*, Vol. 67, No. 6, 3704–3711, Jun. 2019.
27. Roshna, T. K., U. Deepak, and P. Mohanan, "Compact UWB MIMO antenna for tridirectional pattern diversity characteristics," *IET Microwaves, Antennas Propagation*, Vol. 11, No. 14, 2059–2065, 2017.
28. Yang, K., X. Bao, P. McEvoy, and M. J. Ammann, "Pattern reconfigurable back-to-back microstrip patch antenna," *IET Microwaves, Antennas Propagation*, Vol. 10, No. 13, 1390–1394, 2016.
29. Malik, J., A. Patnaik, and M. V. Kartikeyan, "Novel printed MIMO antenna with pattern and polarization diversity," *IEEE Antennas and Wireless Propagation Letters*, Vol. 14, 739–742, 2015.
30. Saraswat, R. K. and M. Kumar, "A frequency band reconfigurable UWB antenna for high gain applications," *Progress In Electromagnetics Research B*, Vol. 64, 29–45, 2015.
31. Saraswat, R. K. and M. Kumar, "Miniaturized slotted ground UWB antenna loaded with metamaterial for WLAN and WiMAX applications," *Progress In Electromagnetics Research B*, Vol. 65, 65–80, 2016.